



OPEN

## Dose reduction potential in cone-beam CT imaging of upper extremity joints with a twin robotic x-ray system

Karsten Sebastian Luetkens<sup>1✉</sup>, Süleyman Ergün<sup>2</sup>, Henner Huflage<sup>1</sup>, Andreas Steven Kunz<sup>1</sup>, Carsten Herbert Gietzen<sup>1</sup>, Nora Conrads<sup>1</sup>, Lenhard Pennig<sup>3</sup>, Lukas Goertz<sup>3</sup>, Thorsten Alexander Bley<sup>1</sup>, Tobias Gassenmaier<sup>1</sup> & Jan-Peter Grunz<sup>1</sup>

Cone-beam computed tomography is a powerful tool for 3D imaging of the appendicular skeleton, facilitating detailed visualization of bone microarchitecture. This study evaluated various combinations of acquisition and reconstruction parameters for the cone-beam CT mode of a twin robotic x-ray system in cadaveric wrist and elbow scans, aiming to define the best possible trade-off between image quality and radiation dose. Images were acquired with different combinations of tube voltage and tube current–time product, resulting in five scan protocols with varying volume CT dose indices: full-dose (FD; 17.4 mGy), low-dose (LD; 4.5 mGy), ultra-low-dose (ULD; 1.15 mGy), modulated low-dose (mLD; 0.6 mGy) and modulated ultra-low-dose (mULD; 0.29 mGy). Each set of projection data was reconstructed with three convolution kernels (very sharp [Ur77], sharp [Br69], intermediate [Br62]). Five radiologists subjectively assessed the image quality of cortical bone, cancellous bone and soft tissue using seven-point scales. Irrespective of the reconstruction kernel, overall image quality of every FD, LD and ULD scan was deemed suitable for diagnostic use in contrast to mLD (very sharp/sharp/intermediate: 60/55/70%) and mULD (0/3/5%). Superior depiction of cortical and cancellous bone was achieved in FD<sub>Ur77</sub> and LD<sub>Ur77</sub> examinations ( $p < 0.001$ ) with LD<sub>Ur77</sub> scans also providing favorable bone visualization compared to FD<sub>Br69</sub> and FD<sub>Br62</sub> ( $p < 0.001$ ). Fleiss' kappa was 0.618 (0.594–0.641;  $p < 0.001$ ), indicating substantial interrater reliability. In this study, we demonstrate that considerable dose reduction can be realized while maintaining diagnostic image quality in upper extremity joint scans with the cone-beam CT mode of a twin robotic x-ray system. Application of sharper convolution kernels for image reconstruction facilitates superior display of bone microarchitecture.

### Abbreviations

CBCT	Cone-beam computed tomography
CTDI <sub>vol</sub>	Volume computed tomography dose index (mGy)
DAP	Dose-area product
FD	Full-dose scan protocol
LD	Low-dose scan protocol
ULD	Ultra-low-dose scan protocol
mLD	Modulated low-dose scan protocol
mULD	Modulated ultra-low-dose scan protocol

Fractures of the upper extremity are associated with individual physical impairment and often high socio-economic relevance. While distal radius fractures are among the most frequent trauma consequences in any emergency department with particularly high incidence in elderly patients<sup>1–3</sup>, dislocations and fractures in the

<sup>1</sup>Department of Diagnostic and Interventional Radiology, University Hospital Würzburg, Oberdürrbacher Straße 6, 97080 Würzburg, Germany. <sup>2</sup>Institute of Anatomy and Cell Biology, University of Würzburg, Koellikerstraße 6, 97070 Würzburg, Germany. <sup>3</sup>Institute for Diagnostic and Interventional Radiology, Faculty of Medicine and University Hospital Cologne, University of Cologne, Kerpener Straße 62, 50937 Cologne, Germany. ✉email: Luetkens\_K@ukw.de



**Figure 1.** Rendering of staff member demonstrating the scan position for 3D cone-beam CT imaging of upper extremity joints using the tableside trajectory of the twin robotic x-ray system.

elbow region are more common in younger populations<sup>4</sup>. Plain radiographs usually represent the primary imaging method if traumatic injuries of the upper limb are suspected<sup>5</sup>. Radiograms offer a compromise between fast scan time, ubiquitous availability, and low radiation dose on the one side, and limited 2D image information on the other side<sup>6</sup>. Considering that trauma mechanisms can be vastly heterogeneous, ranging from simple falls on the outstretched hand from standing height to high-velocity injuries in sports activities and motor vehicle accidents<sup>2,7</sup>, 2D imaging may be insufficient for trauma evaluation in some patients. Especially more severe injuries, e.g., multi-fragmentary, intraarticular and displaced fractures of the wrist and elbow require additional 3D assessment for presurgical planning<sup>8</sup> and image fusion with intraoperative fluoroscopy<sup>9,10</sup>. In addition, computed tomography scans allow for reliable exclusion or detection of radiographically occult fractures in case of divergent clinical presentation<sup>11</sup>. Even for certain chronic conditions or postoperative follow-up imaging, CT can provide valuable diagnostic information with the typical drawback of increased radiation dose<sup>12,13</sup>.

Despite the predominance of multidetector CT in most radiology departments, the value of another technical approach to computed tomography is increasingly recognized for skeletal imaging tasks: Combining a flat-panel detector build with pyramid-shaped beam geometry, cone-beam computed tomography (CBCT) has become a powerful tool for 3D imaging in trauma patients. Detailed visualization of bone microarchitecture<sup>14</sup>, superior positioning options and potential for reduced radiation dose are among the major advantages compared to conventional multidetector CT<sup>15</sup>. Having been considered an integral part of maxillofacial imaging for a long time<sup>16–19</sup>, access to dedicated scanners for the appendicular skeleton has led to increasing relevance of CBCT in musculoskeletal imaging during the last decade<sup>20</sup>.

The twin robotic x-ray system in this study represents a novel approach to the CBCT formula that uses two telescopic arms for 2D and 3D image acquisition instead of a conventional gantry-based approach. Whilst the benefits of the CBCT option for fracture detection have previously been analyzed, data regarding the actual dose reduction potential of this multi-use system is lacking. Therefore, in this work, various combinations of acquisition and reconstruction parameters were evaluated for the CBCT mode of the twin robotic x-ray system in cadaveric wrist and elbow scans, aiming to define the best possible trade-off between image quality and radiation dose.

## Material and methods

**Cadaveric phantoms.** For this experimental study, we received permission from the institutional review board of the University of Würzburg, Germany (IRB number 20200506 01). Two formalin-fixed cadaveric specimens were obtained from the anatomical institute of the local university. Body donors had voluntarily donated their bodies to the anatomical institute for study and scientific purposes. Thus, the ethics committee of the University of Würzburg waived additional written informed consent. Bilateral wrist and elbow examinations were performed for both cadaveric specimens in supine position using the twin robotic x-ray system's tableside scan trajectory. Scanning process for upper extremity imaging is displayed in Fig. 1 by a staff member (informed consent for publication was obtained). All procedures were conducted in accordance with the relevant guidelines and regulations.

**Cone-beam CT scans.** For image acquisition, the multifunctional radiography system (Multitom Rax, Siemens Healthcare GmbH, Erlangen, Germany) uses two telescopic arms connected to ceiling rails within the x-ray suite. One of the arms holds a quadratic flat-panel detector (edge length 426 mm), while the other carries the x-ray tube. Different motion trajectories for both arms allow for 2D and 3D imaging in specified positions. CBCT scans are performed with an asymmetric source-to-image distance of 1150 mm, an input field of  $213 \times 213$  mm<sup>2</sup> and a 2D matrix of  $1440 \times 1440$  un-binned pixels in high-resolution mode, which results in an effective pixel size of 149  $\mu$ m. The current software version VF 11 (Siemens Healthcare GmbH) supports acquisition of 26 projection images per second with a sweep angle of 200 degrees, hence resulting in a total scan time of 14 s.

Before each CBCT scan, system settings can be manually adjusted to achieve target dose levels. Using a clinically established full-dose protocol (FD) as reference, four other scan protocols with lower radiation doses were

Multitom Rax <sup>a</sup>	Full-dose mode	Low-dose mode	Ultra-low-dose mode	Modulated low-dose mode	Modulated ultra-low-dose mode
Reference kVp	80	80	60	80	80
Scan mAs	2.5	0.6	0.5	Regulated	Regulated
DAP (dGy × cm <sup>2</sup> )	54.3	14.0	3.5	Mean 1.9	Mean 0.9
CTDI <sub>vol(16 cm)</sub> (mGy)	17.4	4.5	1.2	Mean 0.6	Mean 0.3
Effective dose (μSv)	13.2	3.4	0.9	Mean 0.5	Mean 0.2
Relative dose	100%	25.8%	6.8%	3.8%	1.5%

**Table 1.** Scan protocols and radiation dose. Operator settings and dose estimation for 3D cone-beam CT examinations with different acquisition protocols. DAP dose-area product, CTDI<sub>vol(16 cm)</sub> volume computed tomography dose index (for 16 cm diameter PMMA dosimetry phantom). <sup>a</sup>Siemens Healthcare GmbH; Erlangen, Germany.

evaluated in this study. Images were either acquired with different fixed combinations of tube voltage and tube current–time product (low-dose [LD], ultra-low-dose [ULD]) or with the scanner’s automatic dose modulation feature (modulated low-dose [mLD], modulated ultra-low-dose [mULD]): In this scan mode, a sensor implemented in the flat-panel detector measures the incoming radiation for each projection image. Dependent on the previously determined dose level, the tube current–time product is then adjusted continuously throughout the acquisition process. Scan parameters and corresponding radiation dose values associated with each CBCT examination protocol are summarized in Table 1. Dose-area products for all examinations were obtained from the automatically created scan report. To calculate volume CT dose indices (CTDI<sub>vol</sub>), multiplication by a linear scaling factor that we computed in advance for every combination of tube current–time product and tube voltage was needed. Therefore, dose-length product measurements were performed in the five chambers of a conventional 16 cm PMMA dosimetry phantom (IEC 60601-2-44:2009 compliant). After standard weighting schemes were applied to obtain volume dose-length product values (DLP<sub>vol(16 cm)</sub>), these values were divided by the field of view in z-direction (equal to the beam width) to compute the CTDI<sub>vol(16 cm)</sub>. Finally, dividing the CTDI<sub>vol(16 cm)</sub> by the DAP resulted in the required scaling factor.

**Reconstruction kernels.** Each set of projection data was reconstructed with dedicated 3D processing software (syngo via, Siemens Healthcare GmbH) using different modulation transfer functions characterized by standard convolution kernels: very sharp (Ur77):  $\rho_{10}=25.4$  lp/cm,  $\rho_{50}=16.7$  lp/cm; sharp (Br69):  $\rho_{10}=15.1$  lp/cm,  $\rho_{50}=12.3$  lp/cm; intermediate (Br62):  $\rho_{10}=11.3$  lp/cm,  $\rho_{50}=9.2$  lp/cm (all Siemens Healthcare GmbH). Reformatting was performed in orthogonal planes (axial, coronal and sagittal) with slice thickness of 1.0 mm, increment of 0.5 mm, image matrix of 1024 × 1024 pixels and field of view of 80 mm. Window settings were 3000 and 1000 Hounsfield units (width and center) by default with observers being allowed to modify the contrast manually on screen for their reads.

**Image analysis.** After image reconstruction, all datasets were analyzed in randomized and blinded fashion with standard picture archiving and communication software (Merlin, Phoenix-PACS, Freiburg im Breisgau, Germany) by five independent radiologists with 8, 7, 6, 5 and 4 years of experience in musculoskeletal imaging. First, each observer was tasked to evaluate whether the reviewed scan was sufficient for diagnostic use. Second, readers assessed overall image quality and gave dedicated image quality ratings for cortical bone, cancellous bone and soft tissue using a seven-point Likert scale (7 = excellent, 6 = very good, 5 = good, 4 = satisfactory, 3 = fair, 2 = poor, 1 = very poor image quality).

**Statistics.** All tests and analyses were conducted using specialized software (SPSS Statistics Version 27 for Mac, IBM, Armonk, New York, USA) with *p* values less than 0.05 indicating statistical significance. Categorical items are reported in form of percentages, frequencies and median values. Wilcoxon signed rank and Friedman tests were carried out to compare two or more paired non-parametric variables. Interrater reliability was assessed by calculation of Fleiss’ kappa with interpretation of agreement following Landis and Koch (1.00–0.81 = almost perfect; 0.80–0.61 = substantial; 0.60–0.41 = moderate; 0.40–0.21 = fair; 0.20–0.00 = slight; < 0.00 = poor agreement)<sup>21</sup>.

## Results

**Dose comparison between scan protocols.** Operating with fixed tube current–time products, CTDI<sub>vol(16 cm)</sub> of low-dose and ultra-low-dose scans was 4.5 and 1.2 mGy, corresponding to 74.2% and 93.1% of dose reduction compared to the standard full-dose scan protocol used in clinical routine (17.4 mGy). With automatic dose regulation activated, modulated low-dose (mean CTDI<sub>vol(16 cm)</sub> 0.6 mGy) and modulated ultra-low-dose acquisition (mean CTDI<sub>vol(16 cm)</sub> 0.3 mGy) allowed for dose reduction of 96.6% and 98.3% (*p* < 0.001). Scan parameters and dose values were equal for wrist and elbow scans.

**Image quality assessment.** Independent of the convolution kernel used for image reconstruction, overall image quality of every FD, LD and ULD scan in this study was deemed suitable for diagnostic evaluation in

	Very sharp	Sharp	Intermediate
<b>Overall image quality</b>			
Full-dose mode	7 (1.00)	6 (1.00)	5 (1.00)
Low-dose mode	6 (1.00)	5 (1.00)	4 (1.00)
Ultra-low-dose mode	3.5 (0.50)	4 (0.58)	3 (0.40)
Modulated low-dose mode	2 (0.13)	2 (0.15)	3 (0.10)
Modulated ultra-low-dose mode	1 (0)	1 (0)	1.5 (0)
<b>Diagnostic image quality</b>			
Full-dose mode	100%	100%	100%
Low-dose mode	100%	100%	100%
Ultra-low-dose mode	100%	100%	100%
Modulated low-dose mode	60%	55%	70%
Modulated ultra-low-dose mode	0%	3%	5%

**Table 2.** Overall image quality assessment. Synopsis of overall image quality evaluation in cadaveric wrist and elbow scans by five radiologists for each combination of convolution kernel and dose protocol. Median rating values and share of examinations with at least “satisfactory” image quality (score  $\geq 4$ ) are reported. Percentage of studies that were deemed “suitable for diagnostic use in patient studies” is displayed.

clinical routine by all five radiologists. In contrast, readers considered 40/45/30% of mLD and 100/97/95% of mULD (Ur77/Br69/Br62 kernel) insufficient for clinical imaging. Comparing reconstructions with the same kernel, studies with higher dose levels produced superior overall image quality in upper extremity scans (all  $p < 0.001$ ). Detailed observer ratings are outlined in Table 2. The best overall image quality was reported for FD<sub>Ur77</sub> examinations (median scale value 7). Evaluation of LD<sub>Ur77</sub> studies delivered favorable results compared to FD<sub>Br62</sub> ( $p < 0.001$ ) and comparable image quality to FD<sub>Br69</sub> scans ( $p = 0.157$ ). No distinction was stated between LD<sub>Br69</sub> and FD<sub>Br62</sub> ( $p = 0.475$ ). For examinations with the ULD scan protocol, at least satisfactory image quality (scale value  $\geq 4$ ) was declared in 50/58/40% of studies with no significant difference between image processing algorithms (median 3.5/4/3;  $p = 0.072$ ). Fleiss’ kappa was 0.618 (95% confidence interval 0.594–0.641;  $p < 0.001$ ), indicating substantial interrater reliability for image quality assessment. Figures 2 and 3 contain representative CBCT images in axial and coronal orientation for visualization of image quality.

Comparing the effect of each convolution kernel on the display of bone microarchitecture, visualization of cortical and cancellous bone was best in very sharp reconstructions of full-dose and low-dose examinations ( $p < 0.001$ ), with LD<sub>Ur77</sub> scans also providing favorable bone depiction compared to FD<sub>Br69</sub> and FD<sub>Br62</sub> ( $p < 0.001$ ). Accordingly, sharper ULD<sub>Ur77</sub> ( $p = 0.005$ ) and ULD<sub>Br69</sub> ( $p = 0.009$ ) reconstructions were deemed more suitable for differentiation of trabecula and fatty marrow than softer ULD<sub>Br62</sub> studies. The effect of the different convolution kernels on image sharpness is exemplified in Fig. 4. Quality of cortex display in ultra-low-dose scans was independent of image processing ( $p = 0.764$ ). For soft tissue analysis, no difference between kernels was identified in full-dose ( $p = 0.302$ ) and low-dose image acquisition ( $p = 0.129$ ). In ultra-low-dose studies, both ULD<sub>Br69</sub> ( $p = 0.008$ ) and ULD<sub>Br62</sub> ( $p < 0.001$ ) provided superior soft tissue assessability compared to ULD<sub>Ur77</sub> with no difference between the two softer kernels ( $p = 0.739$ ). Detailed image quality evaluation for bone and soft tissue is summarized in Table 3.

## Discussion

In this multi-observer study, we evaluated the image quality provided by 15 combinations of acquisition protocols and reconstruction parameters for the CBCT scan mode of a twin robotic x-ray system in cadaveric wrist and elbow imaging. We were able to show that dose reduction of more than 90% is feasible for certain imaging tasks, while maintaining diagnostic image quality with a dedicated ultra-low-dose scan protocol. Reducing the radiation dose even further by implementing detector-based dose modulation resulted in a considerable amount of non-diagnostic studies. Therefore, we postulate that the ultra-low-dose protocol with reduced tube voltage represents the best trade-off between required dose and image assessability for upper extremity scans.

A recent meta-analysis by Nardi et al. identified an average dose of 7.1  $\mu\text{Sv}$  for CBCT scans of the appendicular skeleton, stating considerable dose reduction potential in comparison to multidetector CT imaging<sup>22</sup>. Compared to conventional radiography, however, radiation dose of CBCT remains significantly higher in most studies<sup>23</sup>. While scan protocols without a focus on dose reduction may have the potential to overcome the image quality of state-of-the-art multidetector CT scanners, we believe that CBCT can also challenge radiography as the primary method of fracture diagnosis<sup>24</sup>. Due to distance to the radiation-sensitive body trunk, effective dose of extremity imaging is generally lower than for other body regions<sup>25</sup>. Providing diagnostic 3D image information with approximately four times the effective dose of standard 2D radiograms, the ultra-low-dose protocol in this study appears promising for primary use in particular imaging tasks, e.g., carpal bone<sup>14,23</sup> or radial head evaluation<sup>26</sup>. Furthermore, pediatric radiology could benefit from the reduced radiation dose in cases that require 3D assessment to ascertain the injury pattern, e.g., in distal humerus fractures<sup>26</sup>. To investigate which scan protocol is appropriate for different pathologies should be part of future research. From a technical point of view, the maintained image quality in ultra-low-dose scans may foremost be attributed to the small effective pixel size of 149  $\mu\text{m}$  realized by the combination of asymmetric acquisition geometry (the detector rotates in a



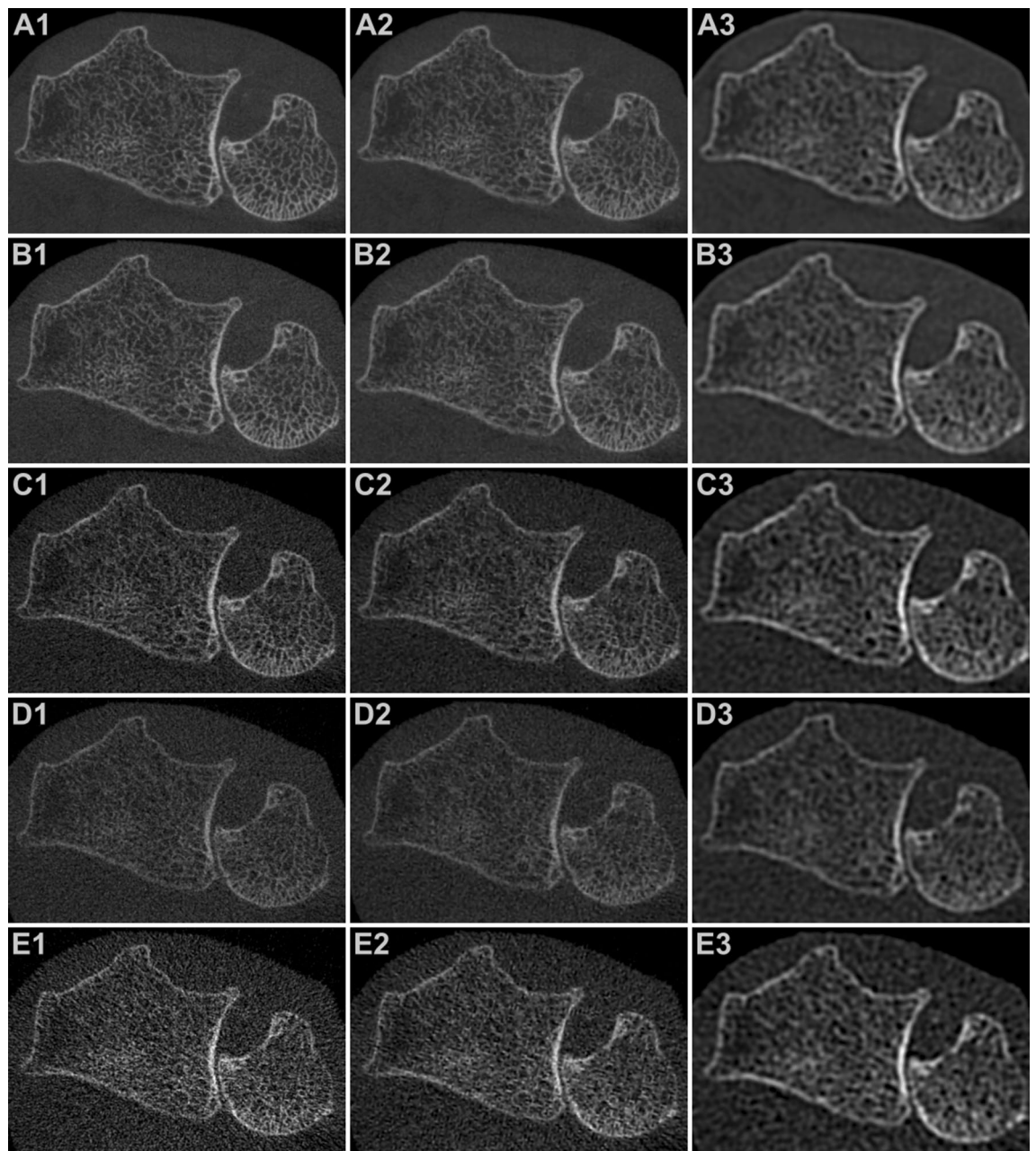


**Figure 2.** Axial reformatted of 3D wrist scans with varying acquisition parameters and reconstruction kernels: **(A)** Full-dose mode (A1: very sharp; A2: sharp; A3: intermediate). **(B)** Low-dose mode (B1: very sharp; B2: sharp; B3: intermediate). **(C)** Ultra-low-dose mode (C1: very sharp; C2: sharp; C3: intermediate). **(D)** Modulated low-dose mode (D1: very sharp; D2: sharp; D3: intermediate). **(E)** Modulated ultra-low-dose mode (E1: very sharp; E2: sharp; E3: intermediate).

smaller radius around the isocenter than the x-ray tube to balance the effect of the focal spot size) and un-binned readout of the flat-panel detector in high-resolution mode.

With very sharp reconstructions of low-dose examinations providing favorable image quality over full-dose scans with softer reformatting, additional dose reduction potential can be realized through image postprocessing. In particular, the superior display of cancellous bone in studies reconstructed with the two sharper convolution kernels may aid fracture assessment due to better discrimination of trabecula and fatty bone marrow. In contrast, the inferior visualization of bone microarchitecture provided by the intermediate convolution kernel might be attributed to the fact that the realized modulation transfer function of this kernel is far below the system's resolution limit without a defined kernel.

**Limitations.** The two formalin-fixed cadaveric specimens were selected without knowledge on body donor age, time of fixation and bone density of the examined wrist and elbow region. Thus, preexisting osteopenia and

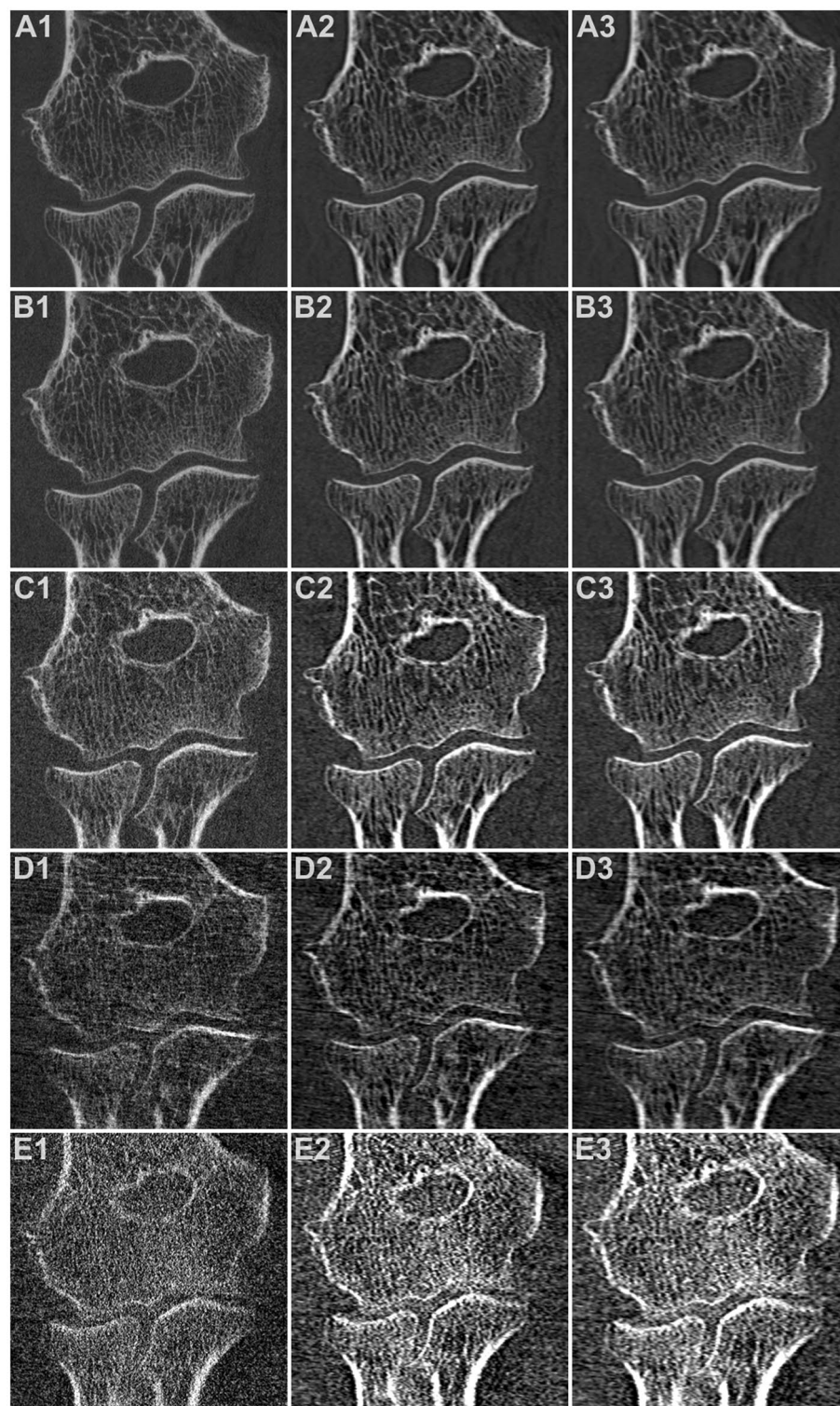


**Figure 3.** Coronal reformatting of 3D elbow scans with varying acquisition parameters and reconstruction kernels: **(A)** Full-dose mode (A1: very sharp; A2: sharp; A3: intermediate). **(B)** Low-dose mode (B1: very sharp; B2: sharp; B3: intermediate). **(C)** Ultra-low-dose mode (C1: very sharp; C2: sharp; C3: intermediate). **(D)** Modulated low-dose mode (D1: very sharp; D2: sharp; D3: intermediate). **(E)** Modulated ultra-low-dose mode (E1: very sharp; E2: sharp; E3: intermediate).



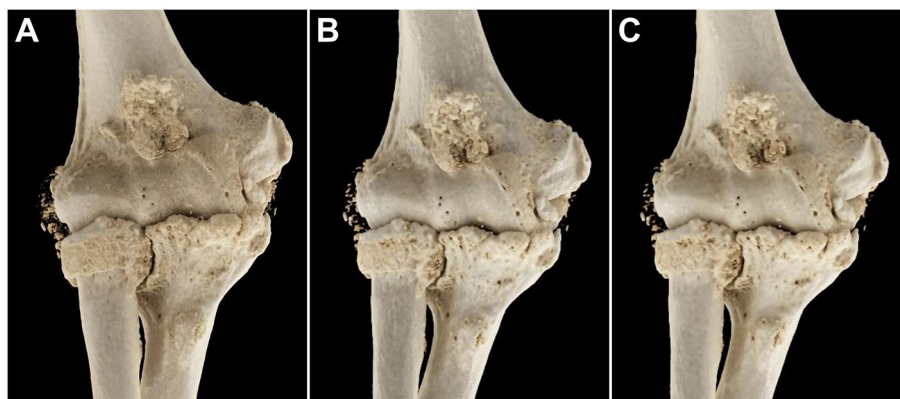


**Figure 4.** Cinematic volume rendering technique (syngo.via, Siemens Healthcare GmbH) demonstrates the difference in image sharpness provided by the three convolution kernels for full-dose elbow studies: (A) Very sharp kernel (Ur77). (B) Sharp kernel (Br69). (C) Intermediate kernel (Br62).

	Very sharp	Sharp	Intermediate
<b>Cortical bone</b>			
Full-dose mode	7 (1.00)	6 (1.00)	5 (1.00)
Low-dose mode	7 (1.00)	6 (1.00)	5 (1.00)
Ultra-low-dose mode	4 (0.50)	4 (0.53)	4 (0.53)
Modulated low-dose mode	3 (0.15)	3 (0.20)	3 (0.35)
Modulated ultra-low-dose mode	1 (0)	1 (0)	1.5 (0)
<b>Cancellous bone</b>			
Full-dose mode	7 (1.00)	6 (1.00)	5 (1.00)
Low-dose mode	6 (1.00)	5.5 (1.00)	4 (1.00)
Ultra-low-dose mode	3.5 (0.50)	4 (0.60)	3 (0.35)
Modulated low-dose mode	2 (0.13)	2 (0.10)	3 (0.05)
Modulated ultra-low-dose mode	1 (0)	1 (0)	1 (0)
<b>Soft tissue</b>			
Full-dose mode	5 (0.80)	4 (0.80)	4 (0.80)
Low-dose mode	4 (0.65)	4 (0.75)	4 (0.65)
Ultra-low-dose mode	2 (0)	2 (0)	2 (0)
Modulated low-dose mode	1 (0)	1 (0)	1.5 (0)
Modulated ultra-low-dose mode	1 (0)	1 (0)	1 (0)

**Table 3.** Detailed image quality assessment for bone and soft tissue. Dedicated image quality evaluation of cortical bone, cancellous bone and soft tissue by five radiologists for each combination of convolution kernel and dose protocol in cadaveric wrist and elbow scans. Median rating values and share of examinations with at least “satisfactory” image quality (score  $\geq 4$ ) are reported.

the demineralizing effect of formalin on bone tissue could have had a negative effect on subjective image quality ratings<sup>27,28</sup>. With examinations in this study limited to cadaveric limbs, the potential effect of motion artifacts in future patient scans could not be estimated. Given the limited number of projection images acquired per scan, the influence of off-center positioning on image quality ought to be evaluated in further studies. However, with motion compensation algorithms continuously improving and comfortable positioning being facilitated by the open scanner architecture, the authors do not expect a considerable loss of image quality in a realistic clinical scenario. Finally, despite being blinded to scan and reconstruction parameters, radiologists could have gained a certain amount of involuntary training during their reading sessions.

## Conclusion

With the cone-beam CT scan mode of a twin robotic x-ray system, dose reduction of more than 90% can be realized for certain upper extremity joint examinations, while maintaining diagnostic image quality. Application of sharper convolution kernels for image reconstruction facilitates superior display of bone microarchitecture, potentially aiding in detection of microfractures in future patient studies.

Received: 5 March 2021; Accepted: 22 September 2021

Published online: 11 October 2021

## References

- Jupiter, J. Future treatment and research directions in distal radius fracture. *Hand Clin.* **28**(2), 245–248 (2012).
- Nellans, K. W., Kowalski, E. & Chung, K. C. The epidemiology of distal radius fractures. *Hand Clin.* **28**(2), 113–125 (2012).
- Shauver, M. J., Yin, H., Banerjee, M. & Chung, K. C. Current and future national costs to medicare for the treatment of distal radius fracture in the elderly. *J. Hand Surg. Am.* **36**(8), 1282–1287 (2011).
- Subasi, M. *et al.* Clinical and functional outcomes and treatment options for paediatric elbow dislocations: Experiences of three trauma centres. *Injury* **46**(Suppl 2), S14–S18 (2015).
- Torabi, M. *et al.* ACR appropriateness criteria(R) acute hand and wrist trauma. *J. Am. Coll. Radiol.* **16**(5S), S7–S17 (2019).
- Guzel, A., Temzioz, O., Aksu, B., Sut, N. & Karasalihoglu, S. A cost analysis of radiologic imaging in pediatric trauma patients. *Ulus. Travma Acil Cerrahi Derg.* **16**(4), 313–318 (2010).
- Porrino, J. A. Jr. *et al.* Fracture of the distal radius: Epidemiology and premanagement radiographic characterization. *AJR Am. J. Roentgenol.* **203**(3), 551–559 (2014).
- Sheehan, S. E., Dyer, G. S., Sodickson, A. D., Patel, K. I. & Khurana, B. Traumatic elbow injuries: What the orthopedic surgeon wants to know. *Radiographics* **33**(3), 869–888 (2013).
- Yoshii, Y., Totoki, Y., Sashida, S., Sakai, S. & Ishii, T. Utility of an image fusion system for 3D preoperative planning and fluoroscopy in the osteosynthesis of distal radius fractures. *J. Orthop. Surg. Res.* **14**(1), 342 (2019).
- Yoshii, Y., Totoki, Y., Tung, W. L., Akita, K. & Ishii, T. A Comparison of radiographic outcomes between 3D preoperative planning and conventional planning in the osteosynthesis of distal radius fractures. *J. Hand Surg. Asian Pac. Vol.* **24**(3), 303–310 (2019).
- Jarraya, M. *et al.* Radiographically occult and subtle fractures: A pictorial review. *Radiol. Res. Pract.* **2013**, 370169 (2013).
- Brenner, D. J. & Hall, E. J. Computed tomography—An increasing source of radiation exposure. *N. Engl. J. Med.* **357**(22), 2277–2284 (2007).
- Goergen, T. *et al.* Chronic elbow pain. American College of Radiology. ACR appropriateness criteria. *Radiology* **215**(Suppl), 339–343 (2000).
- Grunz, J. P. *et al.* Evaluation of ultra-high-resolution cone-beam CT prototype of twin robotic radiography system for cadaveric wrist imaging. *Acad. Radiol.* **28**, e314–e322 (2020).
- Matikka, H. & Viren, T. Radiation dose reduction in cone-beam computed tomography of extremities: Evaluation of a novel radiation shield. *J. Radiol. Prot.* **34**(2), N57–N63 (2014).
- Koong, B. Cone beam imaging: Is this the ultimate imaging modality?. *Clin. Oral Implants Res.* **21**(11), 1201–1208 (2010).
- Roberts, J. A., Drage, N. A., Davies, J. & Thomas, D. W. Effective dose from cone beam CT examinations in dentistry. *Br. J. Radiol.* **82**(973), 35–40 (2009).
- Tsilakakis, K. *et al.* Dose reduction in maxillofacial imaging using low dose cone beam CT. *Eur. J. Radiol.* **56**(3), 413–417 (2005).
- Veldhoen, S. *et al.* Performance of cone-beam computed tomography and multidetector computed tomography in diagnostic imaging of the midface: A comparative study on Phantom and cadaver head scans. *Eur. Radiol.* **27**(2), 790–800 (2017).
- Carrino, J. A. *et al.* Dedicated cone-beam CT system for extremity imaging. *Radiology* **270**(3), 816–824 (2014).
- Landis, J. R. & Koch, G. G. The measurement of observer agreement for categorical data. *Biometrics* **33**(1), 159–174 (1977).
- Nardi, C. *et al.* Radiation dose in non-dental cone beam CT applications: A systematic review. *Radiol. Med.* **123**(10), 765–777 (2018).
- Grunz, J. P. *et al.* Twin robotic x-ray system in small bone and joint trauma: Impact of cone-beam computed tomography on treatment decisions. *Eur. Radiol.* **31**, 3600–3609 (2020).
- Alagic, Z., Bujila, R., Enocson, A., Srivastava, S. & Koskinen, S. K. Ultra-low-dose CT for extremities in an acute setting: Initial experience with 203 subjects. *Skelet. Radiol.* **49**(4), 531–539 (2020).
- Iordache, S. D. *et al.* Radiation exposure from computed tomography of the upper limbs. *Acta Orthop. Belg.* **83**(4), 581–588 (2017).
- Grunz, J. P. *et al.* 3D cone-beam CT with a twin robotic x-ray system in elbow imaging: Comparison of image quality to high-resolution multidetector CT. *Eur. Radiol. Exp.* **4**(1), 52 (2020).
- Burkhart, K. J. *et al.* Influence of formalin fixation on the biomechanical properties of human diaphyseal bone. *Biomed. Tech. (Berl.)* **55**(6), 361–365 (2010).
- Fonseca, A. A., Cherubini, K., Veeck, E. B., Ladeira, R. S. & Carapeto, L. P. Effect of 10% formalin on radiographic optical density of bone specimens. *Dentomaxillofac. Radiol.* **37**(3), 137–141 (2008).

## Author contributions

K.S.L. analyzed and interpreted all data and prepared the manuscript. Observer analysis was performed by K.S.L., A.S.K., H.H., J.P.G. and T.G. C.H.G. and N.C. supported preparation of the manuscript and figures. L.P. and L.G. supported statistical analysis and revised the manuscript. T.A.B. and S.E. contributed to preparation of the manuscript and provided quality control. S.E. also prepared the cadaveric specimens. J.P.G. designed and supervised the study and was a major contributor to the preparation of the manuscript. All authors read and approved the final manuscript.

## Funding

Open Access funding enabled and organized by Projekt DEAL.

## Competing interests

JPG was funded by the Interdisciplinary Center of Clinical Research Würzburg, Germany [grant number Z-2/CSP-06] and serves as a research consultant for Siemens Healthcare GmbH. The Department of Diagnostic and Interventional Radiology received a research grant by Siemens Healthcare GmbH. The authors of this manuscript declare no further relationships with any companies, whose products or services may be related to the subject matter of the article.

## Additional information

**Correspondence** and requests for materials should be addressed to K.S.L.

**Reprints and permissions information** is available at [www.nature.com/reprints](http://www.nature.com/reprints).



**Publisher's note** Springer Nature remains neutral with regard to jurisdictional claims in published maps and institutional affiliations.



**Open Access** This article is licensed under a Creative Commons Attribution 4.0 International License, which permits use, sharing, adaptation, distribution and reproduction in any medium or format, as long as you give appropriate credit to the original author(s) and the source, provide a link to the Creative Commons licence, and indicate if changes were made. The images or other third party material in this article are included in the article's Creative Commons licence, unless indicated otherwise in a credit line to the material. If material is not included in the article's Creative Commons licence and your intended use is not permitted by statutory regulation or exceeds the permitted use, you will need to obtain permission directly from the copyright holder. To view a copy of this licence, visit <http://creativecommons.org/licenses/by/4.0/>.

© The Author(s) 2021